Rational Design, Synthesis, and Characterization of Facilitated Transport Membranes Exhibiting Enhanced Permeability, Selectivity and Stability

Matthew T. Webb[1], Lucas C. Condes[1], Harold G. Ly[1,2],
Michele Galizia[1]*, Sepideh Razavi[1]*

[1] School of Sustainable Chemical, Biological and Materials Engineering, University of Oklahoma, 100 E. Boyd Street, Norman 73019, OK, USA

[2] Oklahoma School of Science and Mathematics (OSSM), 1141 N. Lincoln Blvd, Oklahoma City 73104, OK, USA

Submission to the Journal of Membrane Science

REVISED MANUSCRIPT

* *Corresponding Authors: S. Razavi, srazavi@ou.edu; M. Galizia, mgalizia@ou.edu*

GRAPHICAL ABSTRACT

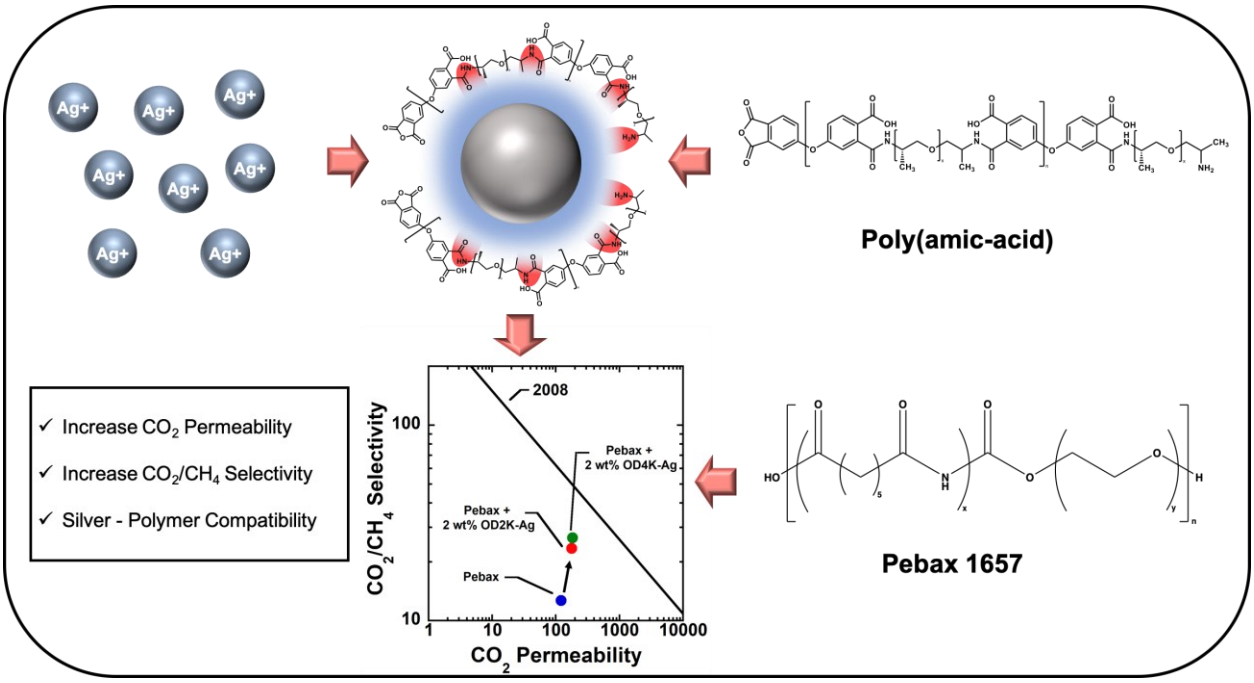

HIGHLIGHTS:

- Silver nanoparticles stabilized with ether containing poly(amic-acid)s exhibit excellent stability.
- Silver nanoparticles stabilized with ether containing poly(amic-acid)s increase Pebax CO_2 permeability by 50% and CO_2/CH_4 selectivity by 100%.
- Tunable CO_2 solubility and diffusivity can be achieved using silver nanoparticles with varying ether groups.

ABSTRACT

Despite outperforming conventional polymer membranes in the short time frame, facilitated transport membranes (FTMs) are prone to photo/chemical aging, which causes a rapid decay of their performance. Moreover, when embedded in polymer materials to fabricate mixed matrix membranes, structural defects may form at the metal-polymer interface, causing a selectivity loss. To overcome these issues, a series of poly(amic acid)s (PAAs) have been synthesized using 4,4'-oxydiphathalic anhydride (ODPA) and Jeffamine monomers of varying molecular weight, and used to fabricate silver nanoparticles via the chelating reaction with silver ions, in attempts to simultaneously *i)* achieve defect-free mixed matrix membranes (MMMs), *ii)* target CO_2 selective transport, and *iii)* enhance long-term stability. The occurrence of the chelating reaction between silver and the PAA was confirmed, and as a result, individual and un-aggregated PAA-coated silver nanoparticles were obtained and incorporated into a commercial polymer, Pebax 1657, to fabricate defect-free mixed matrix membranes. The effect of the PAA length and ether functional group concentration on the structure and performance of the resulting mixed matrix membranes was systematically investigated. Remarkably, inclusion of only 2 wt% nanoparticles in Pebax enhances the CO_2 permeability by 50% and CO_2 selectivity by 100% relative to neat polymer. A detailed analysis of the sorption and diffusion coefficients was performed to elucidate the molecular origin of the observed membrane performance. Finally, preliminary data show that the newly synthesized materials exhibit high chemical stability upon exposure to pure H_2.

Keywords:

Facilitated transport membranes; CO_2 capture; diffusivity-selectivity; solubility-selectivity; stability.

1. INTRODUCTION

Nanoparticles (NPs) are of utmost interest due to their unique chemical-physical properties, which substantially differ from those of bulk materials. The tunable nature of NP properties enables their use in a variety of applications such as optics [1,2,3], electronics [4,5,6], nanomedicine [7,8,9], drug delivery [10], and molecular separations [11,12]. In this last regard, nanoparticles can be embedded in polymer materials to tune their transport properties and achieve superior selectivity/permeability performance in a variety of industrially relevant separations [13,14,15,16,17,18]. Specifically, silver ions/NPs have traditionally been used as facilitated transport carriers for specific gasses, such as carbon dioxide and ethylene [19,20,21]. As recommended by the 2019 NAS report "*A Research Agenda for Transforming Separation Sciences*", achieving high selectivity is the crucial factor to debottleneck membrane-based separations and make them competitive with conventional processes [22]. More in general, current research efforts in the membrane field are oriented towards enhancing selectivity and long-term durability [23,24,25,26,27,28,29,30]. This paper aims at proposing a novel strategy to simultaneously enhance selectivity, permeability and stability in CO_2 separation systems.

Facilitated transport membranes (FTM) have been an active area of research in membrane science, providing materials that far exceed the separation performance of conventional polymer materials and position in the upper-right side of the Robeson upper bound [13,19,31,32]. As shown by Eriksen et al., an ethylene permeability of 26,800 Barrer and a corresponding ethylene/ethane (C_2H_4/C_2H_6) selectivity of 1930 (i.e., > 99.9 wt% ethane purity) was achieved by soaking glycerin-swollen Nafion membranes into an aqueous solution of silver tetrafluororborate ($AgBF_4$) [33]. By comparison, most

membranes have an ethylene permeability between 1 to 1000 Barrer, with a C_2H_4/C_2H_6 selectivity less than 10 [34]. However, due to the instability of the facilitated transport carrier (e.g., reduction of ions), as well as non-selective interfacial polymer-filler defects, these films fall short of commercial viability [13]. As an example, $AgBF_4$ incorporated into poly(2-oxazoline) suffered a 100% decrease in the C_2H_4/C_2H_6 selectivity in as little as 4 hours [35].

Solid-state configurations with fixed carrier sites, which function based on a chained-carrier mechanism, are one avenue towards improving FTMs [36,37,38,39]. In 2015, Zhou et. al. doped Pebax polymer membranes with nanospheres formed by silver NPs chelated with polydopamine, observing a simultaneous increase in CO_2 permeability and CO_2/CH_4 selectivity relative to neat Pebax. Using a 15 wt% loading, the enhanced selectivity experienced an 8% decrease over the span of 7 days [40]. Although these pioneering results look promising, the individual and synergistic contributions from the silver and polymer ligand remain largely unknown. Furthermore, the exploration of different ligands and their effects on the long-term stability and performance of FTMs are crucially important in attempts to further enhance the performance and long-term stability of these systems.

To address the downsides associated with FTMs by use of NPs, it is necessary to carefully consider the design of the particle and its capping agents. Poly(amic-acid)s (PAAs) show favorable carbonyl-silver coordination interactions that ultimately are responsible for the formation of stable silver NPs via the chelating mechanism [41]. Secondly, electron acceptors within PAAs (e.g., carboxylic acids) polarize the particle surface, which helps tune selectivity and offers particle protection from photo/chemical

degradation [36]. Additionally, by applying the solution-diffusion separation principles [42], incorporation of functional groups (i.e., ethers) that interact with target solutes (e.g., CO_2) can further benefit the separation performance of existing membrane systems [43,44,45,46,47]. Finally, improving the NPs compatibility with polymer matrices is expected to inhibit the formation of non-selective defects, thus providing an additional opportunity to enhance selectivity in membrane applications [48,49].

In this study, rationally designed nanoparticles targeting CO_2 separation were synthesized by chelating silver NPs with PAAs. Each PAA was molecularly designed to include polyether segments to target CO_2 transport and achieve particle compatibility in polyether-based membranes. Using a variety of physical, chemical, and structural characterizations, the effect of the PAA on the structure and properties of NPs was systematically investigated. NPs were then incorporated, in the amount of 2 wt%, in Pebax 1657, a commercial polymer of practical interest for CO_2 separation, showing that CO_2 permeability can be enhanced by 50% and CO_2/CH_4 selectivity by 100%. The molecular origin of this behavior was elucidated by breaking permeability into its sorption and diffusion contributions. Finally, the stability of the newly synthesized materials was tested by exposing them to pure H_2 for 24h, after which CO_2 and CH_4 permeability and CO_2/CH_4 selectivity were re-measured. Therefore, the approach proposed in this study provides a unique avenue to achieve high CO_2 selectivity and permeability, while simultaneously prolonging the long-term durability of the ensuing systems.

2. MATERIALS AND METHODS

2.1. Materials. 4,4'-Oxydiphathalic anhydride (ODPA) was purchased from Sigma-Aldrich (97 wt % purity), and two Jeffamine D-series grades, exhibiting molecular weight of 2000 (D2K) and 4000 g/mol (D4K), were generously donated by Huntsman corporation (cf. Table 1). Prior to use, all monomers (i.e., Jeffamine and ODPA) were dried under vacuum for 24 hours at room temperature and stored in a desiccator. The PAA reaction medium, tetrahydrofuran (THF), was purchased from Fisher chemical with a water content of 0.02 %. The water content was further reduced using 3Å molecular sieves purchased from Sigma-Aldrich, for at least 24 hours. Methanol (>99 %), which was used to remove monomer/oligomers from the synthesized polymers, was purchased from Acros Organics. Deuterated chloroform, $CDCl_3$, to be used for nuclear magnetic resonance (NMR) characterization, was purchased from Cambridge Isotope Laboratories, Inc. (99.8%). Ethylene glycol (EG), to be used as the reducing agent in the NP synthesis, was purchased from Fisher chemical. The NP precursor, silver nitrate ($AgNO_3$), was purchased from Acros Organics with a purity >99 %. Chloroform ($CHCl_3$) was purchased from Sigma-Aldrich to extract the NPs from EG and to dissolve Pebax 1657 for membrane fabrication. Ultrapure water with an in-line resistivity of 18.2 MΩ-cm, used throughout the study, was produced via a MilliQ7000 purification system. White mineral oil with a flash point of 360-400 °F, to be used to control the reaction temperature, was obtained from Fischer Scientific. Pebax 1657 was purchased from Arkema to serve as the membrane bulk material. 200 proof ethanol (ETOH) was purchased from Fisher Chemical to dissolve Pebax for membrane fabrication via solution casting.

2.2 Synthesis Techniques

2.2.1 Synthesis of Poly(amic-acid). The PAAs were synthesized through a nucleophilic substitution reaction by Jeffamine's amine group at one of ODPA's anhydride carbonyl carbons (cf. Figure 1). This reaction was performed in a 100 ml three-neck flask, manufactured by Chemglass, equipped with a Lab Fish mechanical stirrer and a water jacketed reflux column. A nitrogen blanket was first provided to the flask to remove any traces of humidity. The flask was then charged with 30 ml of THF and 15 mmol of Jeffamine [50]. The same procedure was used for both Jeffamines, D2K or D4K.

Table 1: Summary of Diamines Used in This Study.

Name	*Abbreviation*	*Molecular Weight (g/mol)*	*Chemical Structure*	*X*	*Resultant Polymer Abbreviation*
Jeffamine D2000	*D2K*	*2000*	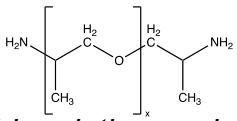	*33*	*OD2K*
Jeffamine D4000	*D4K*	*4000*		*68*	*OD4K*

Listed is the diamine commercial name, its abbreviation, molecular weight, structure, the number of internal repeated units (X), and the abbreviations used for the PAA resulting from the reaction between ODPA and each diamine.

The mixture was stirred at room temperature until homogeneous. Then, the solution was cooled to 0 ºC using an ice bath before adding 15 mmol of ODPA. The purpose of the ice bath during the initial monomer consumption was to improve the molecular weight of the resulting PAA, given the exothermic nature of the reaction [51]. The initial attack of the amine on the anhydride carbonyl occurs rapidly, within the first few minutes of the reaction. After 10 minutes, the flask was heated on a hot plate to 30 ºC using a bath of white mineral oil. The mixture was allowed to react for three hours to ensure a high

molecular weight polymer was formed, capable of passivating the silver surface quickly in the NP synthesis. Following this step, the PAA was precipitated using a methanol/water (10/90 vol%) mixture and subsequently rinsed using this mixture over a vacuum filtration device. This step was done to remove any unreacted monomers and oligomers. The resulting PAAs (OD2K/OD4K) (cf. Figure 1 and Figure S1, Supporting Information) were dried under vacuum for 24 hours at room temperature and stored in a chemical refrigerator at 4 ºC. The PAA derived from ODPA and D2K will be abbreviated by OD2K, while the PAA derived from ODPA and D4K will be abbreviated by OD4K.

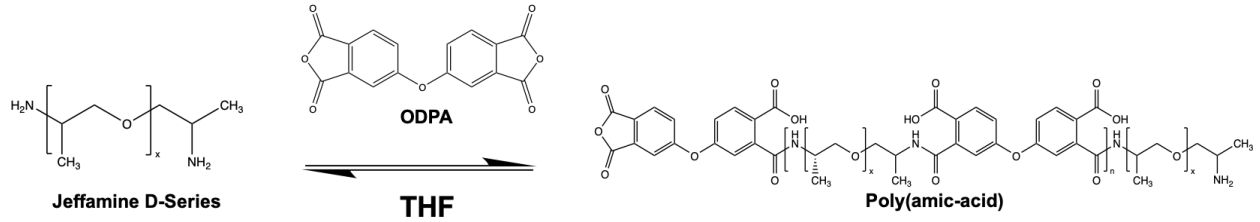

Figure 1*: Reaction between Jeffamine and ODPA for the synthesis of Poly(amic-acid) (PAA) in THF. The resulting PAA structure is shown. X denotes the number of repeating segments within each Jeffamine molecule (cf. Table 1). N denotes the number of repeating segments within the overall PAA.*

2.2.2 Synthesis of Silver Nanoparticles. The NP synthesis was performed in a 100 ml three-neck flask from Chemglass equipped with a magnetic stirrer, water jacketed reflux column, and a nitrogen blanketed atmosphere. First, 200 mg of either OD2K or OD4K was added to the flask and completely dissolved in 40 ml of EG (cf. Figure 2, Step 1) This mixture was heated to 100 ºC on a hot plate using a mineral oil bath. $AgNO_3$ was dissolved in a separate beaker using ultrapure water at a concentration of 40 wt%, following the procedure by Kim *et al* [52]. 2 ml of this aqueous solution was rapidly injected into the flask using a syringe to induce particle nucleation (cf. Figure 2, Step 2). The

resulting concentration of $AgNO_3$ after addition to the reaction volume was 0.5 M. The reaction was maintained at 100 ºC for 30 minutes, allowing time for particle growth. At this time, the solution was quickly cooled down to room temperature using a water bath at 20 ºC (cf. Figure 2, Step 3). To denote the particle type in an abbreviated manner, Ag is added to the end of the PAA that was used in the synthesis (e.g., OD2K-Ag are silver NPs synthesized using OD2K).

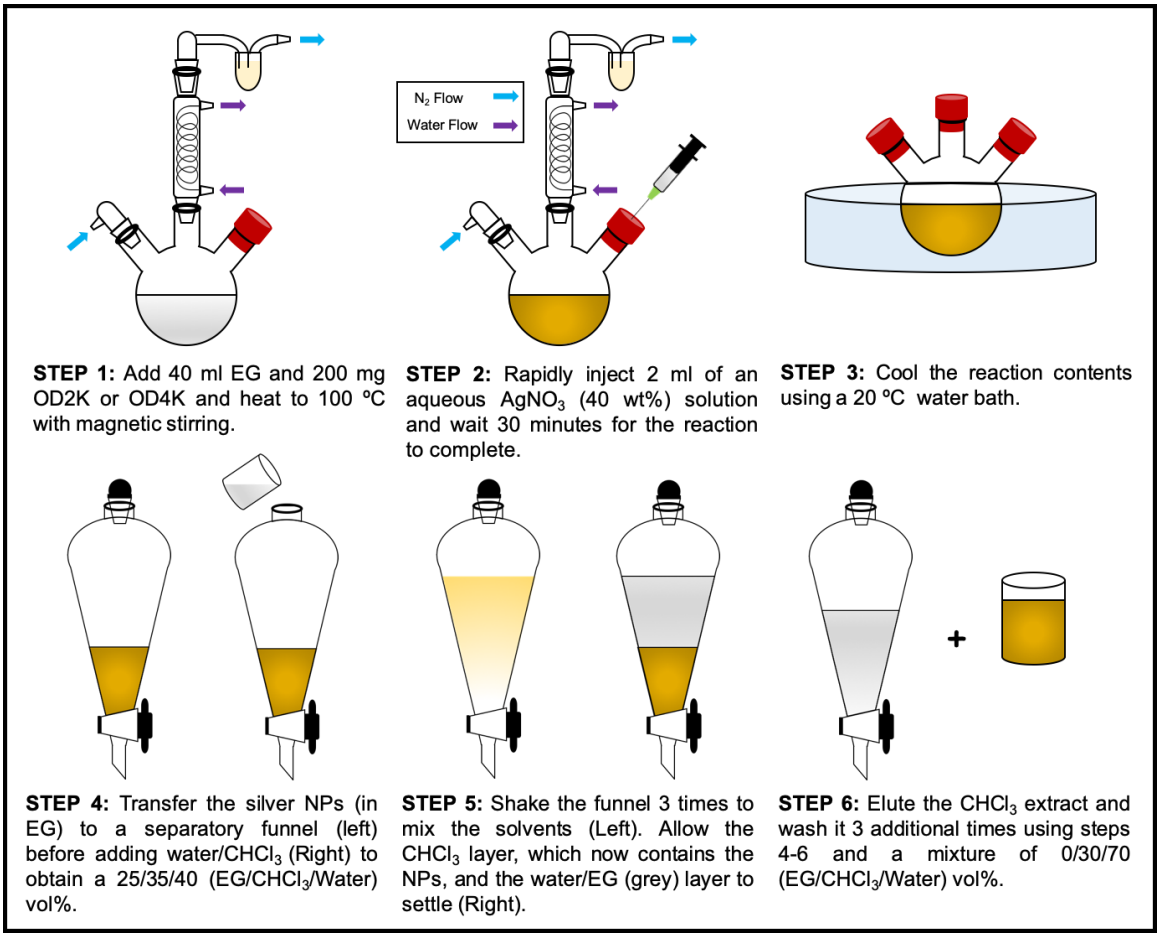

Figure 2: *Schematic of the silver nanoparticle synthesis.*

The nascent particles, still in EG, were then transferred to a 500 ml separatory funnel and mixed with $CHCl_3$ at a 40/60 (EG/$CHCl_3$) vol% ratio (cf. Figure 2, Step 4). The particles were pushed from EG into the $CHCl_3$ layer upon adding ultrapure water, at a vol% ratio of ~25/35/40 for EG/$CHCl_3$/H_2O, respectively. Likewise, EG was selectively removed by the aqueous layer. NPs were placed in chloroform, rather than remaining in EG, to facilitate their subsequent dispersion in polymers to fabricate the mixed matrix membranes. Such choice is based on: *i)* chloroform's immiscibility with the aqueous phase to facilitate the extraction process, *ii)* chloroform's similarity of solubility parameter to the silver NP's steric polymer layer ($CHCl_3$ – 19 $MPa^{0.5}$, EG – 32.9 $MPa^{0.5}$, and OD2K/OD4K ~ 20.2/19.7 $MPa^{0.5}$, cf. SI section 1 and 6) and *iii)* the lower boiling point of $CHCl_3$ (61 ºC) relative to EG (197 ºC). The funnel was shaken several times before allowing the solvent layers to settle (cf. Figure 2, Step 5). The $CHCl_3$ phase was removed, and the funnel was cleaned before adding the $CHCl_3$ extract back into the funnel (cf. Figure 2, Step 6). The $CHCl_3$ phase was then rinsed 3 additional times in the separatory funnel using ultrapure water at a 30/70 ($CHCl_3$/H_2O) vol % ratio. Between each wash, the $CHCl_3$ extract was removed, and the funnel was cleaned. The final particle suspension in $CHCl_3$ was placed in PTFE lined amber vials and stored in a refrigerator at 4 ºC.

2.2.3 Mixed Matrix Membranes Fabrication

Neat Pebax membranes were fabricated via the solution-casting of a 2.5 wt% solution in ETOH/$CHCl_3$ (50/50 vol%), which was dissolved at 50 ºC. Both OD2K-Ag and OD4K-Ag were used to fabricate composite materials with Pebax by adding a prescribed amount of particles to the polymer solution. The final silver concentration in these

materials was targeted around 2 wt%. Since the particles are also suspended in chloroform, the solvent composition used to dissolve Pebax was slightly altered, so as to obtain a final mixture of Pebax and particles that was 50/50 vol% (ETOH/$CHCl_3$). This was done to ensure that the total volume and composition of the mixture remained constant. Each mixture was sonicated for 5 minutes before being poured onto a leveled glass dish at room temperature and inside a nitrogen filled glove bag, to prevent samples oxidation. The samples were allowed to dry for 3 days prior to use. The membrane thickness was measured using a Mitutoyo micrometer ten times, with values ranging between 80-100 μm. Membranes containing 2 wt% OD2K-Ag and OD4K-Ag are referred to as Pebax+2OD2K-Ag and Pebax+2OD4K-Ag respectively.

2.3. Characterization Methods

2.3.1 Nuclear Magnetic Resonance (NMR). OD2K and OD4K were characterized by ^{1}H NMR analysis using a VNMRS 500MHz-NMR spectrometer. Prior to the synthesis of OD2K and OD4K, D2K, D4K, and ODPA were examined using NMR to ensure that no impurities were present. Deuterated chloroform ($CDCl_3$) (99.8%, Cambridge Isotope Laboratories) was used as the solvent with a polymer concentration of 2 wt%. ^{1}H NMR spectra were referenced internally to $CDCl_3$ (δ = 7.26 ppm).

2.3.2 Fourier Transform Infrared Spectroscopy (FTIR). OD2K, OD4K, OD2K-Ag, and OD4K-Ag were analyzed using a Nicolet iS50R Fourier Transform Infrared Spectroscope (FT-IR) in the iS50 attenuated total reflectance (ATR) mode using 64 scans with a resolution of 0.4821 cm^{-1} (cf. Supporting Information, Section 2).

2.3.3 Dynamic light scattering (DLS). was used to measure the effective hydrodynamic diameter of OD2K and OD4K in various solvents, in attempt to corroborate the solubility parameter calculated using the group contribution method (cf. Section 1 in the Supporting Information). These measurements were performed on a NanoBrook Series Particle Analyzer using backscattered detection. For more information, cf. Section 6 of the Supporting Information.

2.3.4 Transmission Electron Microscopy (TEM). Micrographs of the OD2K-Ag and OD4K-Ag were obtained using a JEOL 2000FX transmission electron microscope (TEM) at 200kV with LaB_6 electron source. 20 µL of a silver NP suspension in $CHCl_3$ (~500 PPM) was dropped onto a 3mm copper grid with a carbon support film. The particle size distribution and morphology were determined based on 160 NPs, using Fiji image analysis [53].

2.3.5 Ubbelohde Viscometer. The intrinsic viscosity of OD2K and OD4K was found using a size 0C Ubbelohde viscometer purchased from Cannon Instruments, calibrated with a viscometer constant of 0.003309 cSt/s^2. The intrinsic viscosity was used to compare relative molecular sizes. OD2K and OD4K were prepared at concentrations ranging from 0.3 to 1 g dL^{-1} in $CHCl_3$ and tested at 35 ºC. The reduced viscosity (η_{red}) and inherent viscosity (η_{inh}) were measured at each concentration five times (cf. Figure S4 Supporting Information). The intrinsic viscosity for OD2K and OD4K were determined by averaging the extrapolated value for the η_{red} and η_{inh} at a concentration of 0 g dL^{-1} (cf. section 3 of the Supporting Information). This relative trend was then compared to molecular weight estimates obtained from gel permeation chromatography measurements.

2.3.6 Gel Permeation Chromatography (GPC). Using a Waters 717 plus auto sampler, 30 µL of a 0.1 w/w% polymer solution in $CHCl_3$ was injected into a 7.5 x 250 mm Agilent polypore column at a flowrate of 1 ml/min and at 40 ºC. The eluent was detected using a Waters 490E programmable multi-wavelength detector, set to 260 nm. Details surrounding the weight calculations, as well as the overall molecular weight distribution of OD2K and OD4K is available in section 4 of the Supporting Information.

2.3.7 Thermogravimetric Analysis (TGA). TGA was used to individuate mass losses for OD2K, OD4K, OD2K-Ag, OD4K-Ag, Pebax, Pebax+2OD2KAg, and Pebax+2OD4K-Ag. About 10-20 mg (dry mass) of each sample was placed into a TA Instruments TGA Q500 under nitrogen gas, flowing at 10 ml/min. In the case of the silver NPs (OD2K-Ag and OD4K-Ag), which are suspended in $CHCl_3$, the TGA pan was first filled dropwise with the liquid. The $CHCl_3$ was allowed to evaporate, and the addition was repeated until sufficient particle dry mass was obtained. The samples were heated at a rate of 10 ºC /min from 28 to 800 ºC, and any mass losses were recorded. First and second derivative analysis was used to determine temperature ranges of individual mass loss events (cf. Figure S6-S8, Supporting Information). TGA was coupled with GPC and TEM information to calculate the polymer surface grafting density (σ) as follows [54]:

$$\sigma = \frac{N_A\left(\frac{g_{pol}}{g_{Ag}}\right)\rho_{Ag}r}{3M_n} \qquad \text{(Eq. 1)}$$

where N_A is Avogadro's number (6.022×10^{23} chains mol^{-1}), g_{pol} is the polymer mass, g_{Ag} is the silver mass, r is the equivalent radius of the nanoparticle (based on TEM measurements, cf. Figure 6 and Table 3), and ρ_{Ag} is the density of the silver

nanoparticles, which was assumed to be nearly identical to that of bulk silver (i.e., 10.5 g cm^{-3}). Each TGA measurement exhibited an uncertainty of 5 %.

2.3.8 Scanning Electron Microscopy (SEM). Scanning electron micrographs of Pebax, Pebax+2OD2K-Ag, and Pebax+2OD4K-Ag's cross-section were used to characterize structure morphology. Cross-sections were prepared by fracturing each sample after immersion in liquid nitrogen. Prior to imaging, each sample was sputter coated with iridium. Images were taken using a ThermoFisher Quattro device at 10 kx, with an accelerating voltage of 10 KeV.

2.3.9 Pure gas sorption and permeability measurements. Pure gas (CH_4 and CO_2) permeability was measured at 1 bar and 35 ºC and pure gas solubility (CH_4 and CO_2) was measured from 5 to 20 bar at 35 ºC. Details about these measurements are provided in section 7 of the Supporting Information. Gas diffusivities were estimated using the solution diffusion model:

$$\overline{D} = \frac{P}{S} \qquad \text{(Eq. 2)}$$

where P is the permeability, S is the solubility coefficient, and $\overline{D}$ is the concentration averaged diffusion coefficient. The ideal (i.e., pure-gas) CO_2/CH_4 selectivity (α^P) was estimated as shown in Eq. 3 and broken into its sorption (α^S) and diffusion (α^D) contributions:

$$\alpha^P = \frac{P_{CO_2}}{P_{CH_4}} = \frac{S_{CO_2}}{S_{CH_4}} \times \frac{D_{CO_2}}{D_{CH_4}} = \alpha^S \times \alpha^D \qquad \text{(Eq. 3)}$$

2.3.10 Stability Testing. Both Pebax+2OD2K-Ag and Pebax+2OD4K-Ag, were exposed to 1 atm H_2 at 35 °C for 24 hours. Pure gas CH_4 and CO_2 permeability were measured at 1 atm and 35 °C before and after exposure to H_2. Changes in CO_2

permeability and CO_2/CH_4 selectivity as a result of H_2 exposure are shown and compared in Table 4.

3. RESULTS AND DISCUSSION

3.1. Poly(amic-acid) Characterizations. FTIR was used to provide evidence that the PAA was formed. Figure 3A shows the FTIR spectra of the synthesized OD2K compared to ODPA and D2K, while Figure 3B shows the FTIR spectra of the synthesized OD4K compared to ODPA and D4K in the wavelength range 1500 and 1900 cm^{-1}. The spectral features in this region show key changes in the carbonyl groups during the reaction, providing insight to the polymerization.

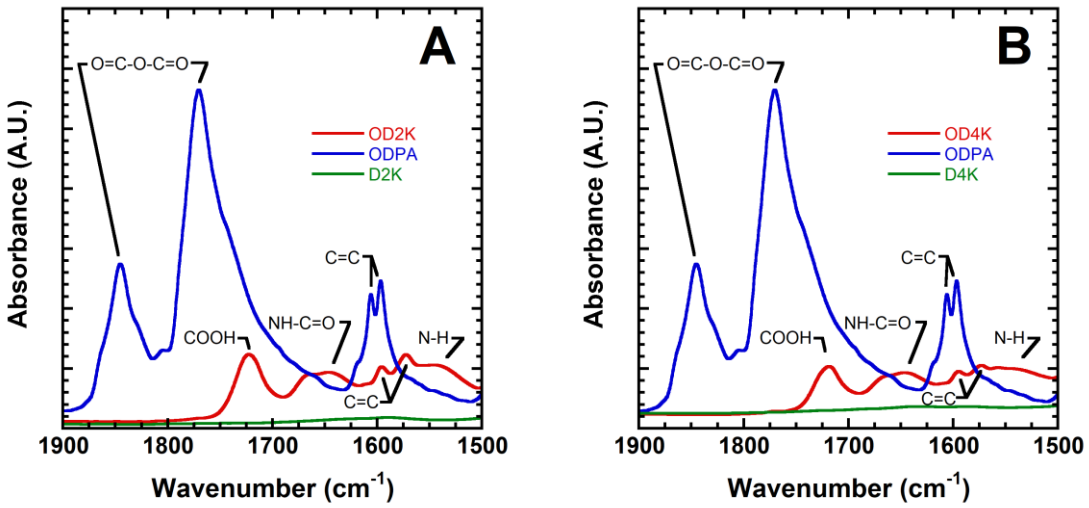

Figure 3: *A) ATR-FTIR spectra of the synthesized OD2K sample compared with the ODPA and D2K reactants, between 1500 and 1900 cm^{-1} wavenumbers. B) ATR-FTIR spectra of the synthesized OD4K sample compared with the ODPA and D4K reactants, between 1500 and 1900 cm^{-1} wavenumbers.*

The D2K and D4K samples exhibited low absorption in this region in contrast to the spectrum obtained for ODPA. ODPA has characteristic peaks at 1770 and 1846 cm^{-1}, which are representative of the symmetric and asymmetric stretching of the anhydride carbonyl, respectively [55]. The loss of these peaks in both OD2K and OD4K's spectra indicates that the reactants are being mostly consumed by the reaction and removed by subsequent washings. The formation of the amic-acid group is supported by the appearance of peaks at 1655 and 1545 cm^{-1} that correspond to the Amide I (C=O stretching) and II (N-H bending) bands for a secondary amide [56]. Additionally, a peak at 1723 cm^{-1} shows the simultaneous appearance of the carboxylic acid carbonyl [55]. Finally, there is a clear red shift (i.e., a shift of around 10 cm^{-1} towards lower wavenumbers) in the aromatic alkene bonds from ODPA to its incorporation into the polymer due to the mesomeric effect [56].

^{1}H NMR can further describe the results of the reaction by confirming the retention of basic reactant structures. In the ^{1}H NMR spectra of both OD2K (cf. Figure 4A) and OD4K (cf. Figure 4B), the main chain proton signals for aromatic protons of the dianhydride, aliphatic protons of the diamine, and terminating/side chain methyl groups appeared around 7-8, 3-4.5, and 1-1.5 ppm, respectively [57]. This is an indication that each of the three groups are retained from the reactants after the synthesis.

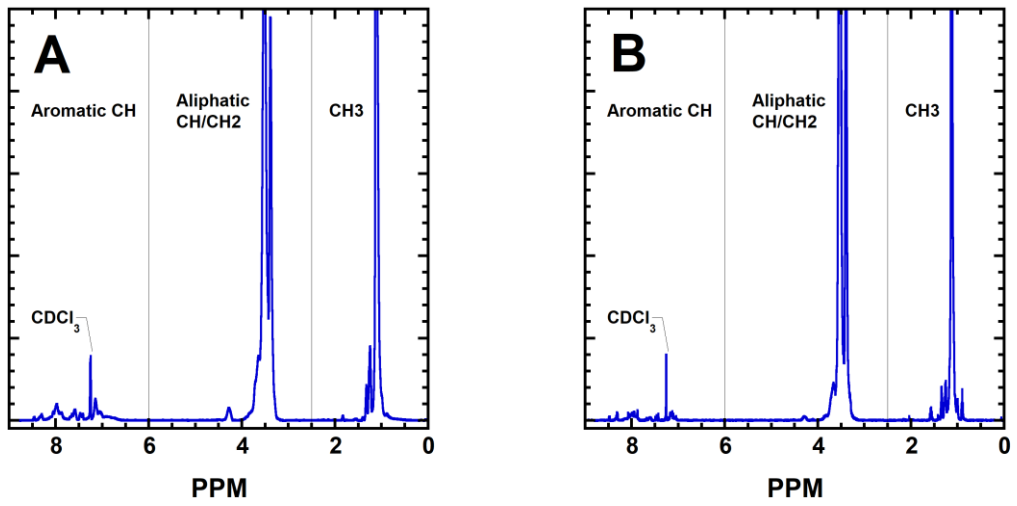

Figure 4: *A) ^{1}H NMR Spectra of OD2K at 2 wt% in $CDCl_3$. B) ^{1}H NMR Spectra of OD4K at 2 wt% in $CDCl_3$.*

The intrinsic viscosities of OD2K and OD4K in $CHCl_3$ at 35 ºC were 0.232 ± 0.001 and 0.255 ± 0.001 dL g^{-1}, respectively (cf. Table 2). The higher value of intrinsic viscosity exhibited by OD4K highlights its larger molecular weight relative to OD2K [58]. These results were corroborated with GPC data, which provided number average molecular weights of 20800 ± 4310 and 42800 ± 8890 g/mol for OD2K and OD4K, respectively (cf. Table 2). Although it appears that, on average, OD4K is nearly twice the projected (i.e., linear) length of OD2K, the two polymers are chemically similar. This is also shown via their solubility parameter, which was calculated using group contribution methods (cf. Section 1 of the Supporting Information) [59]. Based on this method, the solubility parameter of OD2K is 20.2 ± 0.3 MPa$^{0.5}$ and of OD4K is 19.7 ± 0.3 MPa$^{0.5}$. This similarity was also observed by DLS measurements of OD2K and OD4K in a variety of organic solvents, which suggested that both OD2K and OD4K has a solubility parameter around

20 $MPa^{0.5}$, as shown in Figure S9, Supporting Information. Therefore, the two independent measurements provide, within the experimental uncertainty, consistent results. Polymers should experience the greatest swelling in a solvent they are most similar to, and both polymers' hydrodynamic radii experienced a maximum in acetone, whilst OD4K was larger (2.5 nm) compared to OD2K (1.7 nm) (cf. Figure S9, Supporting Information) [58].

Table 2: Summary of OD2K/OD4K Intrinsic Viscosity, Molecular Weight, and Solubility Parameter.

Name	*Intrinsic Viscosity (dL/g)*	*Number Average Molecular Weight (g/mol)*	*Solubility Parameter ($MPa^{0.5}$)*
OD2K	*0.232 ± 0.001*	*20800 ± 4310*	*20.2 ± 0.3*
OD4K	*0.255 ± 0.001*	*42800 ± 8890*	*19.7 ± 0.3*

Listed for OD2K and OD4K is the Intrinsic Viscosity (dL g^{-1}), measured in $CHCl_3$ at 35°C, the number average molecular weight (g mol^{-1}) obtained from GPC experiments, and the solubility parameter based on the group contribution method [34].

3.2. Silver Nanoparticles Characterizations. The formation of PAA-stabilized silver NPs was first verified by examining the FTIR absorption spectra of the NPs. To investigate the interaction that leads to stabilized silver NPs, FTIR was compared between the neat OD2K and the silver nanoparticles modified using OD2K (i.e., OD2K-Ag). As shown in Figure 5A, there is a clear red shift for the carboxylic acid carbonyl stretch from 1722 to 1715 cm^{-1} and for the amide carbonyl peak from 1645 to 1630 cm^{-1}. The red shifting of both carbonyls suggests that they are interacting with the silver surface.

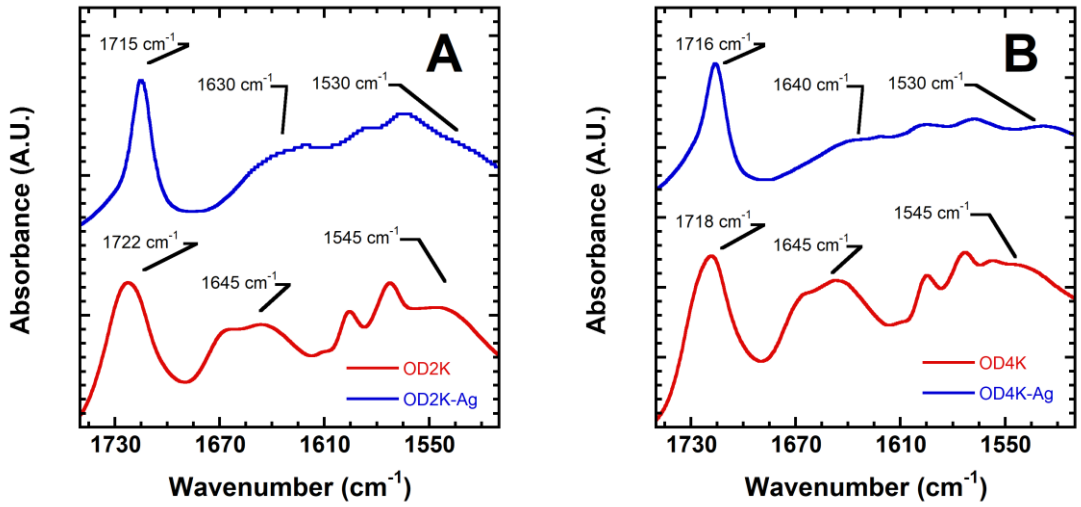

Figure 5: *A) ATR-FTIR spectra of OD2K and the silver nanoparticles stabilized by OD2K (OD2K-Ag) between 1510 and 1750 cm^{-1} wavenumbers. B) ATR-FTIR spectra of OD4K and the silver nanoparticles stabilized by OD4K (OD4K-Ag) between 1510 and 1750 cm^{-1} wavenumbers.*

This is likely due to the ability of the carbonyl lone electron pairs to complex with cationic silver ions located on the NP surface [60]. The amide, in its neutral state, is capable of forming adducts with metal ions at the carbonyl oxygen, but the amide nitrogen is incapable of coordinating with the NP surface without first substituting its hydrogen by deprotonating [61]. Given the poor acidity of secondary amides, this seems unlikely. Instead, shifting in the amide N-H bending from 1545 to 1530 cm^{-1} is more likely due to the positive charge placed on the nitrogen atom as a result of the chelation occurring at the amide carbonyl [61]. Thus, the shifting would be due to the strengthening of mesomeric effects. All other peaks do not experience shifts upon stabilization of silver NPs. A similar comparison was done for OD4K and OD4K-Ag with analogous results (cf.

437 Figure 5B). Through this mechanism, OD2K and OD4K coordinate with the silver NPs to
438 form a protective layer that sterically hinders the NP aggregation. This picture was
439 confirmed by the TEM analysis, as shown in Figure 6.
440
441

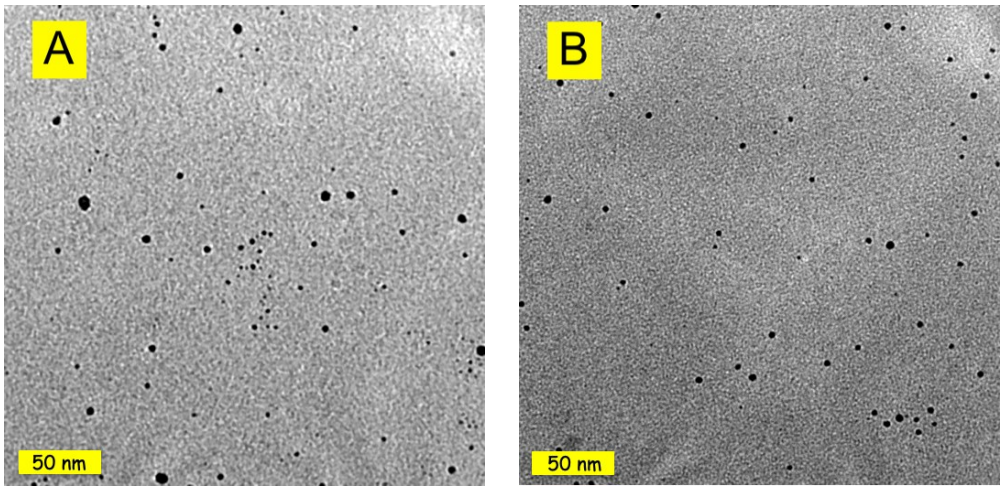

442
443 **Figure 6:** *TEM micrographs (A) OD2K-Ag and (B) OD4K-Ag, imaged at 250kX*
444 *magnification.*
445
446

447 The OD2K-Ag and OD4K-Ag particles are well dispersed and mainly spherical in shape,
448 with equivalent diameters of 6.2 ± 2.9 nm and 4.5 ± 2.5 nm, respectively (cf. Figure 6 and
449 Table 3). Previous studies featuring facilitated transport of olefins, used NPs with
450 diameters less than 30 nm [62]. The much lower NPs size obtained in this study, which
451 leads to an increased particle surface-to-volume ratio, is expected to benefit the
452 transport/separation properties, as shown later in this paper. Even though the molecular
453 weight of OD2K and OD4K were different, stable nanoparticles exhibiting similar size and
454 morphology were achieved. To further investigate any potential differences between the

surface properties of the resulting nanoparticles, thermogravimetric analysis (TGA) was used (cf. Figure 7A/B).

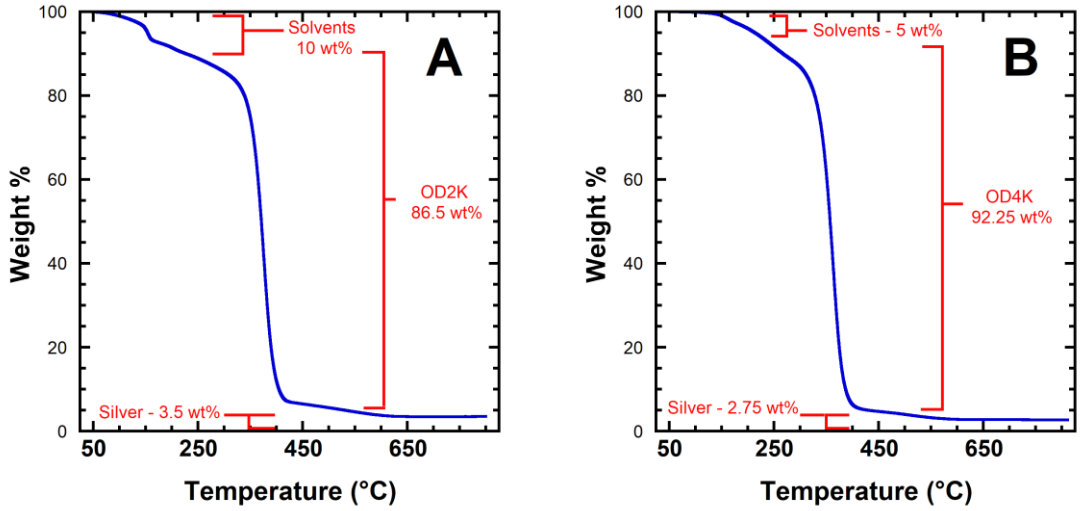

Figure 7: *TGA analysis illustrating the mass loss of A) OD2K-Ag and B) OD4K-Ag, between 28 and 800 ºC.*

Two main mass loss events occur for both particle types. Using first and second derivative analysis (cf. Section 5, Supporting Information), the first mass loss on both curves occurs between 100 and 200 ºC. This is most likely from residual solvents, such as ethylene glycol. The second mass loss occurs between 300 and 450 ºC, which corresponds to the main chain degradation in OD2K and OD4K. The residual mass at 800 ºC is attributed to silver. The overall silver to polymer mass ratio was 4 and 2.9% for OD2K-Ag and OD4K-Ag, respectively (cf. Table 3). The similar mass ratios are consistent within the limit of increasingly smaller particles, whereas the amount of polymer mass needed to surround each particle becomes near constant [63]. Using these values and Eq. 1, the surface grafting density of OD2K-Ag particles is calculated to be 7.6 chains/nm^2, which is approximately twice the estimated value of 4.2 chains/nm^2 for OD4K-Ag particles. Using

473 the surface grafting density and polymer molecular weights, OD4K-Ag nanoparticles
474 contain ~10% more ether groups relative to OD2K-Ag nanoparticles.
475 Despite the similarity in the particle silver/PAA mass ratio (4 for OD2K-Ag and 2.9 for
476 OD4K-Ag), the grafting density of OD2K-Ag (7.6 chains/nm^2) is almost twice that of
477 OD4K-Ag (4.2 chains/nm^2). Mathematically, the shift from a similar mass ratio to different
478 grafting density is based on the molecular weights, which also differ by a factor of ~2
479 (OD4K – Mw = 42800 g/mol; OD2K – Mw = 20200 g/mol). However, a more detailed
480 explanation can be found from Benoit et al. [54]. In that paper, the surface grafting of
481 thiolated polyethylene glycol (PEG) on the surface of gold nanoparticles was analyzed as
482 a function of the PEG molecular weight. When polymer molecular weight increases, the
483 probability of entanglement and chain overlap increases. As a result, when attempting to
484 graft longer chains onto a particle surface, entanglements and added steric hindrance
485 may hamper the efficient packing of polymer chains to the nanoparticle, thus lowering the
486 effective surface grafting density [54]. It should also be noted that particle surface
487 curvature plays a role. On highly curved surfaces (i.e., smaller particles), confinement
488 impacts surface grafting by limiting attachment sites, while also influencing polymer chain
489 conformation and orientation on the particle surface. For both these reasons, it is
490 reasonable to expect a lower grafting density for OD4K-Ag, relative to OD2K-Ag.
491
492
493
494
495

Table 3: Summary of Silver Nanoparticle Size, Composition, and Surface Grafting Density

Name	*Equivalent Diameter (nm)*	*Ag/Polymer Mass Ratio (%)*	*Grafting Density (Chains nm^{-2})*
OD2K-Ag	*6.2 ± 2.9*	*4.0 ± 0.2*	*7.6 ± 2.0*
OD4K-Ag	*4.5 ± 2.5*	*2.9 ± 0.2*	*4.2 ± 0.9*

Listed for each NP is the equivalent diameter (nm), silver (Ag) to polymer mass ratio (%), and PAA polymer surface grafting density (chains/nm^2)

3.3. Mixed Matrix Membrane Structural Characterization. Both OD2K-Ag and OD4K-Ag were incorporated in Pebax at a loading of 1.73 ± 0.09 and 2.06 ± 0.10 wt% silver, respectively, as calculated via TGA measurements (cf. Figures S11 and S12, Supporting Information). Neat Pebax 1657 and its mixed matrix membranes (i.e., Pebax+2OD2K-Ag and Pebax+2OD4K-Ag) exhibit similar thermal stability, with a degradation onset starting at about 300 ºC (cf. Figures S11 and S12, Supporting Information). This finding is consistent with the very low NPs loading.

Scanning electron micrographs showed no signs of structural defects in the Pebax-NPs mixed matrix membranes, thus demonstrating excellent Pebax-NPs compatibility at this loading (cf. Figures 8A-C).

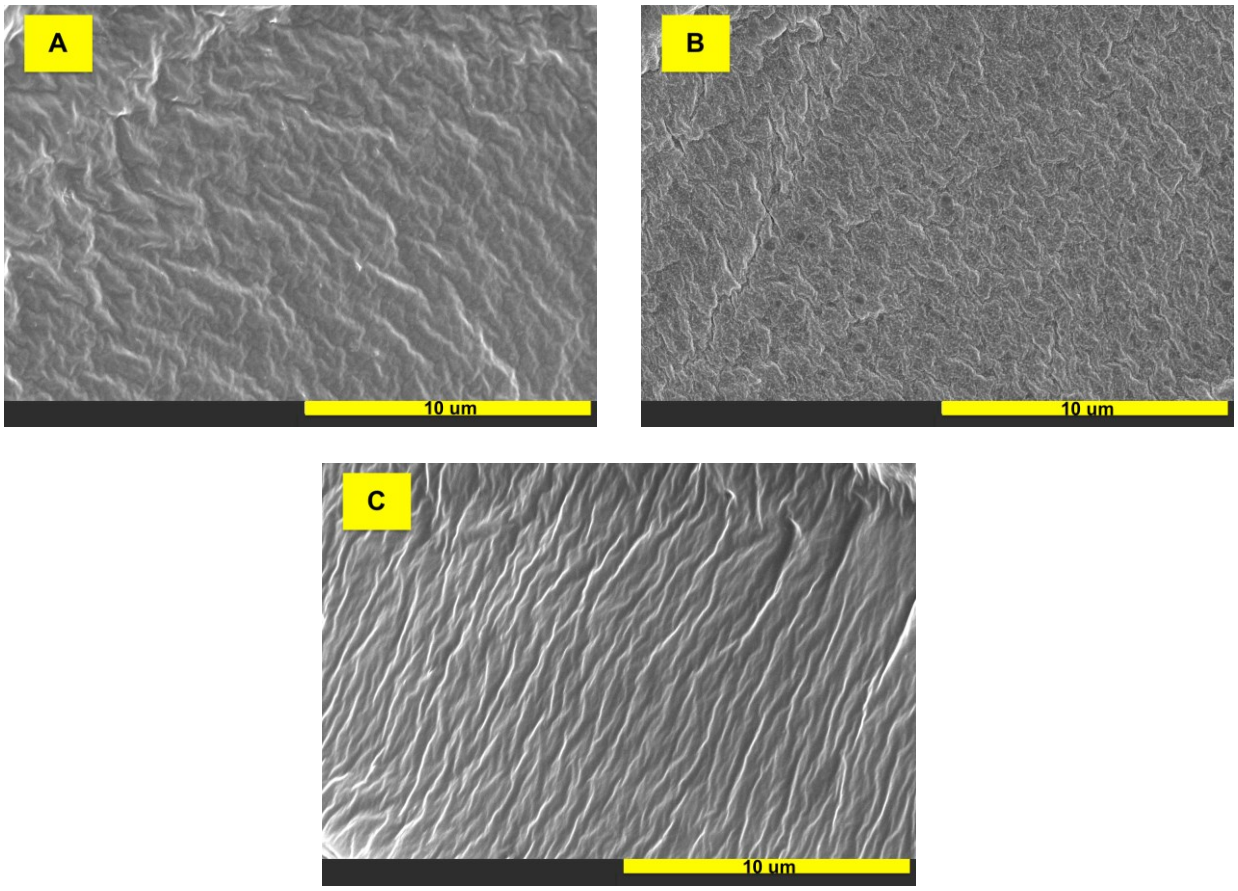

Figure 8: *SEM micrographs for the cross-section of a) Pebax, b) Pebax+2OD2K-Ag, c) Pebax+2OD4K-Ag at 10 kx and 10KeV.*

3.4. Membrane Transport Properties. CO_2 and CH_4 sorption and permeability data in neat Pebax, which were collected to serve as a baseline in this study, exhibit good agreement with literature data [64, 65]. Pure gas sorption isotherms, as well as diffusion and permeability coefficients, are shown in section 7 of the Supporting Information. Experimental uncertainties were estimated via the error propagation method [66]. Upon incorporating OD2K-Ag in Pebax 1657, CO_2 permeability at 35°C and 1 atm increased by 46.8% while CO_2/CH_4 ideal selectivity increased by 84.8% relative to the neat Pebax (cf.

Figure 9A). Similarly, incorporation of OD4K-Ag in Pebax 1657 increased CO_2 permeability by 51.1% and CO_2/CH_4 ideal selectivity by 109.6% relative to neat Pebax (cf. Figure 9A).

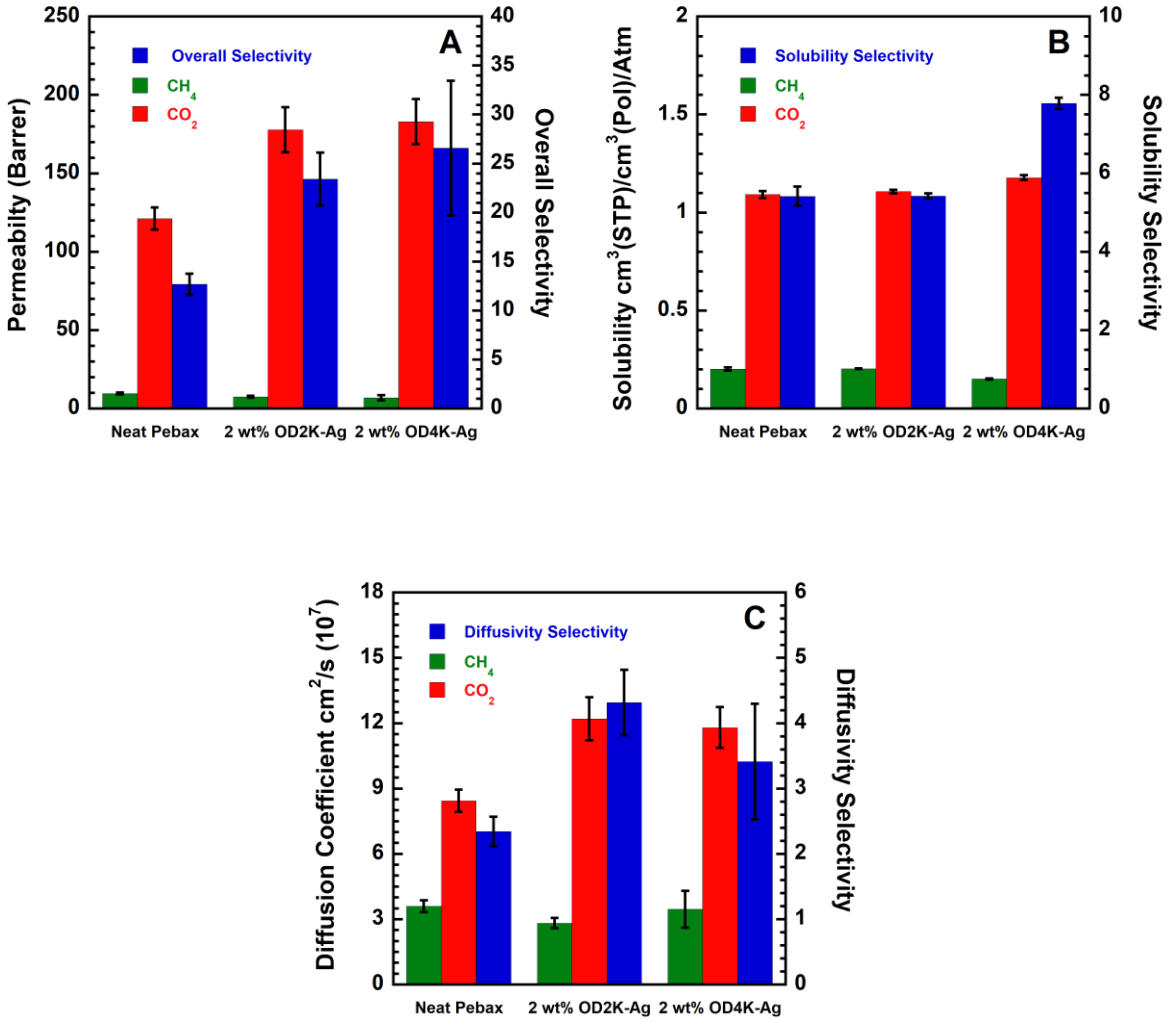

Figure 9. *A) Permeability and CO_2/CH_4 ideal selectivity, B) solubility and CO_2/CH_4 solubility-selectivity, and C) diffusivity and CO_2/CH_4 diffusivity-selectivity in Pebax 1657,*

Pebax + 2OD2K-Ag, and Pebax + 2OD4K-Ag. Data are at 35°C and 1 atm. Error bars were estimated via the error propagation method [66].

To elucidate the molecular origin of the resulting transport behavior, the overall permeability coefficient and selectivity were deconvoluted into their elementary sorption and diffusion contributions. Solubility and solubility-selectivity showed no significant change in Pebax+2OD2K-Ag compared to neat Pebax 1657 (cf. Figure 9B). However, in the case of Pebax+2OD4K-Ag, CO_2 solubility increased by around 8%, whereas solubility-selectivity increased 43.8% compared to neat Pebax 1657 (cf. Figure 9B). This result suggests that the higher ether concentration in OD4K-Ag particles, about 10% above that of OD2K-Ag, could be playing a role in dictating CO_2 solubility changes. Both mixed matrix membranes experienced an impressive increase in CO_2 diffusivity (~40%) and CO_2/CH_4 diffusivity-selectivity (>50%) relative to neat Pebax 1657 (cf. Figure 9C). This physical picture is compatible with CO_2 transport being facilitated by the NPs, while the diffusion of CH_4 occurs via the standard solution-diffusion mechanism. Interestingly, the CH_4 diffusion coefficient slightly decreases upon incorporation of silver NPs with respect to neat Pebax, suggesting that the NPs might increase the tortuosity of the diffusion pathway travelled by CH_4 in the mixed matrix membrane. This effect, however, is within the experimental uncertainty. A summary of transport data at 1 atm and 35°C is shown in Table S4, Supporting Information.

To put the performance of Pebax+2OD2K-Ag and Pebax+2OD4K-Ag in broad perspective, the ideal CO_2/CH_4 selectivity was plotted in a Robeson-type plot as a function of CO_2 permeability and compared with other materials [67-70] (cf. Figure 10), as well as

568 the 2008 upper bound [67]. The simultaneous increase in CO_2 permeability and CO_2/CH_4
569 selectivity shifts both Pebax+2OD2K-Ag and Pebax+2OD4K-Ag closer to the upper
570 bound, relative to the neat Pebax. For example, Pebax+2OD2K-Ag and Pebax+2OD4K-
571 Ag possess similar pure-gas selectivity as Matrimid, cellulose acetate and polysulfone,
572 while its pure-gas CO_2 permeability is about 35 times larger. This enhancement is quite
573 impressive, considering that it can be achieved with a NPs loading of 2% or less.

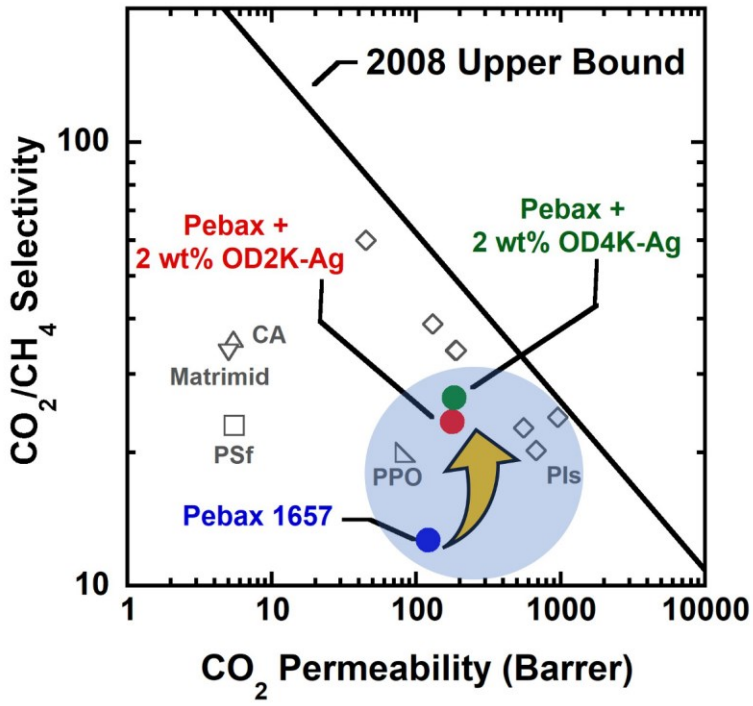

574

575 **Figure 10:** *Comparison among the CO_2/CH_4 separation performance of Pebax,*
576 *Pebax+2OD2K-Ag, and Pebax+2OD4K-Ag with state-of-the-art materials and the 2008*
577 *upper bound [67]. Data are from pure-gas permeation measurements at 35 ºC with a feed*
578 *pressure of 1-10 atm. PSf stands for polysulfone [68], CA stand for cellulose acetate [69],*
579 *PIs stands for polyimides [67], and PPO stands for poly(2,4-dimethly-1,4-phenylene*
580 *oxide) [70].*

Obviously, an important question concerns the long-term stability of these membranes. It is well known, indeed, that silver is prone to reduction/oxidation processes in the presence of UV light and poisoning gasses, such as H_2 and H_2S, which are common contaminants in natural gas. This very important aspect is discussed in detail in section 3.5.

3.5 Membrane Stability. Despite their high performance in the short time-frame, metal ion carriers usually experience photo/chemical ageing, which causes a decay of their performance within a few hours [14,19]. To evaluate the stability of the newly synthesized materials, CO_2 and CH_4 permeability, and CO_2/CH_4 selectivity in Pebax+2OD2K-Ag and Pebax+2OD4K-Ag was measured before and after exposure to H_2 at 1 atm and 35 ºC for 24 hours (cf. Table 4).

Table 4: CO_2 permeability and CO_2/CH_4 selectivity before and after 24-hour hydrogen exposure.

sample	*CO_2 permeability Pre-H_2 (Barrer)*	*CO_2/CH_4 Selectivity*	*CO_2 permeability Post-H_2 (Barrer)*	*CO_2/CH_4 Selectivity*	*% Change in CO_2 Permeability*	*% Change in CO_2/CH_4 Selectivity*
Pebax+2OD2K-Ag	*177.7 ± 9.0*	*25.8 ± 1.9*	*163.3 ± 8.3*	*24.3 ± 1.05*	*-8.8 %*	*-6.0 %*
Pebax+2OD4K-Ag	*187.6 ± 6.5*	*27.6 ± 1.8*	*171.9 ± 6.9*	*25.4 ± 2.9*	*-9.1 %*	*-8.5 %*

Listed for each MMM is the CO_2 permeability (Barrer) and CO_2/CH_4 selectivity, measured at 1 atm and 35 ºC, before and after a 24-hour H_2 exposure at 1 atm and 35 ºC. The percent change in both permeability and selectivity values is included.

The CO_2 permeability in Pebax+2OD2K-Ag before and after H_2 treatment are 177.7 ± 9.0 and 163.3 ± 8.3 Barrer, respectively. Upon exposure to H_2, CO_2 permeability apparently dropped by nearly 9%, with a subsequent drop in CO_2/CH_4 selectivity of 6% (cf. Table 4). However, if we consider the experimental uncertainty affecting these measurements, these drops are negligible; therefore, permeability and selectivity remained essentially

604 unchanged, pointing out the superb stability of the mixed matrix membranes under study
605 to H_2. Similarly, CO_2 permeability and CO_2/CH_4 selectivity in Pebax+2OD4K-Ag
606 experienced an apparent drop of 9.1% and 8.5%, respectively. Again, if we consider the
607 experimental uncertainty (cf. Table 4), this drop is negligible, indicating a very good
608 stability also in the case of Pebax+2OD4K-Ag.
609 Remarkably, after exposure to pure H_2, the overall CO_2 permeability and CO_2/CH_4
610 selectivity remained 40% and 95% higher, respectively, relative to neat Pebax. For the
611 sake of comparison, previously reported Pebax-based facilitated transport membranes
612 containing 80 wt% $AgBF_4$ have experienced a loss in selectivity of higher than 10% after
613 24 hours of H_2 exposure, with a complete loss in selectivity after 30 days [71], indicating
614 that our approach offers not only a simultaneous increase in permeability and selectivity,
615 but also a good stability enhancement. Moreover, the possibility to achieve such
616 enhancement with a very modest NPs loading, only 2% instead of 80% wt, would benefit
617 the economics of the process and, specifically, the investment costs.
618 The analysis of the individual and synergistic effects of the NPs composition, surface
619 grafting density, and weight loading on i) long-term (i.e., >30 days) NP photochemical
620 stability under various conditions (i.e., H_2 and UV), ii) compatibility with the bulk
621 membrane matrix, iii) CO_2 solubility-selectivity and iv) facilitated transport are underway
622 and will be reported in detail in a forthcoming contribution.
623

624 ## 4. CONCLUSIONS

625 Silver NPs were rationally designed using an appropriate polymeric ligand (i.e.,
626 capping agent) to be incorporated in polymers and fabricate novel facilitated transport

membranes (FTMs) exhibiting enhanced CO_2 permeability, CO_2 selectivity and long-term stability. The synthesis of the capping agent, poly(amic-acid, PAAs) was performed through the polycondensation reaction of 4,4'-Oxydipthalic anhydride (ODPA) and Jeffamines exhibiting systematically varied molecular weight (i.e., ether concentration). The polymer structures were confirmed using NMR and ATR-FTIR. The degree of polymerization was similar in polymers containing each diamine, and the impact of the resulting differences in the overall molecular weight with respect to the silver NP synthesis showed little dependence [63]. The particles exhibited clear coordination interactions (i.e., chelation) with the PAAs carbonyl moieties, which produced individual spherical NPs. Micrographs revealed that particles with similar size/morphology were achievable despite the differences in polymer molecular weight. Though, there exist clear differences in the surface grafting density. Once incorporated into Pebax 1657, both NPs produced an impressive increase in overall CO_2 permeability (+50%) and CO_2/CH_4 selectivity (+100%), with increases, in the case of Pebax+2OD4K-Ag, in both CO_2 solubility and diffusivity. These improvements are remarkable, as they were achieved with a very low NPs loading, just 2% or less. Similar or even lower improvements were previously achieved with loadings as high as 80%wt. Equally important, preliminary results indicate that our membranes exhibit high stability upon exposure to H_2, highlighting the importance of rational molecular design of the capping agent. The impact of surface grafting composition, weight loading, as well as the stability of these materials in a variety of environments will be the subject of a forthcoming dedicated contribution.

■ ACKNOWLEDGEMENTS

This work was supported by the Nation Science Foundation through Awards CBET-2005282 (Interfacial Engineering). Partial support from the FIP program (Faculty Investment Program, University of Oklahoma) is also acknowledged. The authors thank Dr. Susan Nimmo, Dr. Julian Sabisch, and Dr. Preston Larson for their training for NMR and microscopy analyses. The authors also thank undergraduate students Ryan Crist, Jordan Vetal, Matthew Casey and Emily Michalak for their experimental collaboration. Finally, Huntsman corporation is acknowledged for generously donating the Jeffamine monomers.

■ REFERENCES

[1] L. Wang, M. Hasanzadeh Kafshgari, M. Meunier, Optical Properties and Applications of Plasmonic-Metal Nanoparticles, Advanced Functional Materials. 30 (2020) 2005400. https://doi.org/10.1002/adfm.202005400.

[2] Y.-X. Zhang, Y.-H. Wang, Nonlinear optical properties of metal nanoparticles: a review, RSC Advances. 7 (2017) 45129–45144. https://doi.org/10.1039/c7ra07551k.

[3] A.N. Shipway, E. Katz, I. Willner, Nanoparticle Arrays on Surfaces for Electronic, Optical, and Sensor Applications, Chemphyschem. 1 (2000) 18–52. https://doi.org/10.1002/1439-7641(20000804)1:1<18::aid-cphc18>3.0.co;2-l.

[4] Y. Li, Y. Wu, B.S. Ong, Facile Synthesis of Silver Nanoparticles Useful for Fabrication of High-Conductivity Elements for Printed Electronics, Journal of the American Chemical Society. 127 (2005) 3266–3267. https://doi.org/10.1021/ja043425k.

[5] L. Nayak, S. Mohanty, S.K. Nayak, A. Ramadoss, A review on inkjet printing of nanoparticle inks for flexible electronics, Journal of Materials Chemistry C. 7 (2019) 8771–8795. https://doi.org/10.1039/c9tc01630a.

[6] A. Kamyshny, S. Magdassi, Conductive Nanomaterials for Printed Electronics, Small. 10 (2014) 3515–3535. https://doi.org/10.1002/smll.201303000.

[7] M. Murphy, K. Ting, X. Zhang, C. Soo, Z. Zheng, Current Development of Silver Nanoparticle Preparation, Investigation, and Application in the Field of Medicine, Journal of Nanomaterials. 2015 (2015) 1–12. https://doi.org/10.1155/2015/696918.

[8] M. Hofmann-Amtenbrink, D. W. Grainger, H. Hofmann, Nanoparticles in medicine: Current challenges facing inorganic nanoparticle toxicity assessments and standardizations, *Nanomedicine: Nanotechnology, Biology and Medicine.* 11 (2015) 1689–1694. https://doi.org/10.1016/j.nano.2105.05.005.

[9] L. Zhang, F. Gu, J. Chan, A. Wang, R. Langer, O. Farokhzad, Nanoparticles in Medicine: Therapeutic Applications and Developments, Clinical Pharmacology & Therapeutics. 83 (2008) 761–769. https://doi.org/10.1038/sj.clpt.6100400.

[10] De Jong, Drug delivery and nanoparticles: Applications and hazards, International Journal of Nanomedicine. (2008) 133. https://doi.org/10.2147/ijn.s596.

[11] D. Sýkora, V. Kašička, I. Mikšík, P. Řezanka, K. Záruba, P. Matějka, V. Král, Application of gold nanoparticles in separation sciences, Journal of Separation Science. 33 (2010) 372–387. https://doi.org/10.1002/jssc.200900677.

[12] Y. Liu, J. Zhang, X. Tan, High Performance of PIM-1/ZIF-8 Composite Membranes for O2/N2 Separation, ACS Omega. 4 (2019) 16572–16577. https://doi.org/10.1021/acsomega.9b02363.

[13] Y. Yampolskii, I. Pinnau, B. Freeman, *Materials Science of Membranes for Gas and Vapor Separation*, Wiley, 2006.

[14] M. Rezakazemi, A. E. Amooghin, M. M. Montzer-Rahmati, A. F. Ismail, T. Matsuura, State-of-the-art membrane based CO_2 separation using mixed matrix membranes (MMMs): An overview on current status and future directions. Progress in Polymer Science. 39 (2014) 817-861. https://doi.org/10.1016/j.progpoylmsci.2014.01.003

[15] M. Moaddeb, W. J. Koros, Gas transport properties of thin polymeric membranes in the presence of silicon dioxide particles. Journal of Membrane Science. 125 (1997) 143-163. https://doi.org/10.1016/S0376-7388(96)00251-7

[16] J. A. Thompson, K. W. Chapman, W. J. Koros, C. W. Jones, S. Nair, Sonication-induced Ostwald ripening of ZIF-8 nanoparticles and formation of ZIF-8/polymer composite membranes. Microporous and Mesoporous Materials. 158 (2012) 292-299. https://doi.org/10.1016/j.micromeso.2012.03.052

[17] T.C. Merkel, Z. He, I. Pinnau, B.D. Freeman, P. Meakin, A.J. Hill, Effect of Nanoparticles on Gas Sorption and Transport in Poly(1-trimethylsilyl-1-propyne), Macromolecules. 36 (2003) 6844–6855. https://doi.org/10.1021/ma0341566.

[18] S. Matteucci, V. A. Kusuma, D. Sanders, S. Swinnea, B. D. Freeman, Gas transport in TIO_2 nanoparticle-filled poly(1-trimethysilyl-1-propyne). Journal of Membrane Science. 307 (2008) 196-217. https://doi.org/10.1016/j.memsci.2007.09.035

[19] L. Cheng, G. Liu, W. Jin, Recent advances in facilitated transport membranes for olefin/paraffin separation, Discover Chemical Engineering. 1 (2021). https://doi.org/10.1007/s43938-020-00001-4.

[20] M. N. Davenport, C. L. Bentley, J.F. Brennecke, B. D. Freeman. Ethylene and ethane transport properties of hydrogen-stable Ag^+-based facilitated transport membranes, Journal of Membrane Science. 647 (2022) Article 120300. https://doi.org/10.1016/j.memsci.2022.120300

[21] W.S. Ho, D.C. Dalrymple, Facilitated transport of olefins in Ag^+-containing polymer membranes, Journal of Membrane Science. 91 (1994) 13-25. https://doi.org/10.1016/0376-7388(94)00008-5

[22] National Academics of Science, Engineering, and Medicine, Division on Earth and Life Sciences, Board on Chemical Sciences and Technology, Committee on a Research

Agenda for a New Era in Separation Science, *A Research Agenda for Transforming Separation Science*, National Academies Press, 2019.

[23] L. M. Robeson, Z. P. Smith, B. D. Freeman, D. R. Paul, Contributions of diffusion and solubility selectivity to the upper bound analysis for glassy gas separation membranes. Journal of Membrane Science. 453 (2014) 71-83. https://doi.org/10.1016/j.memsci.2013.10.066

[24] J. Deng, Z. Huang, B. J. Sundell, D. J. Harrigan, S. A. Sharber, K. Zhang, R. Guo, M. Galizia, State of the art and prospects of chemically and thermally aggressive membrane gas separations: Insights from polymer science. Polymer. 229 (2021) Article 123988. https://doi.org/10.1016/j.polymer.2021.123988

[25] M. Galizia, W.S. Chi, Z.P. Smith, T.C. Merkel, R.W. Baker, B.D. Freeman, 50th Anniversary Perspective: Polymers and Mixed Matrix Membranes for Gas and Vapor Separation: A Review and Prospective Opportunities, Macromolecules. 50 (2017) 7809–7843. https://doi.org/10.1021/acs.macromol.7b01718.

[26] E.-S. Jang, J. Kamcev, K. Kobayashi, N. Yan, R. Sujanani, S.J. Talley, R.B. Moore, D.R. Paul, B.D. Freeman, Effect of Water Content on Sodium Chloride Sorption in Cross-Linked Cation Exchange Membranes, Macromolecules. 52 (2019) 2569–2579. https://doi.org/10.1021/acs.macromol.8b02550.

[27] W. J. Box, Z. Huang, R. Guo, M. Galizia, The mechanism of light gas transport through configurational free volume in glassy polymers, Journal of Membrane Science. 656 (2022) 12608. https://doi.org/10.1016/j.memsci.2022.120608

[28] S. Luo, Q. Zhang, L. Zhu, H. Lin, B.A. Kazanowska, C.M. Doherty, A.J. Hill, P. Gao, R. Guo, Highly Selective and Permeable Microporous Polymer Membranes for Hydrogen Purification and CO2Removal from Natural Gas, Chemistry of Materials. 30 (2018) 5322–5332. https://doi.org/10.1021/acs.chemmater.8b02102.

[29] M. Omidvar, C.M. Stafford, H. Lin, Thermally stable cross-linked P84 with superior membrane H2/CO2 separation properties at 100 °C, Journal of Membrane Science. 575 (2019) 118–125. https://doi.org/10.1016/j.memsci.2019.01.003.

[30] B. Comesaña-Gándara, J. Chen, C.G. Bezzu, M. Carta, I. Rose, M.-C. Ferrari, E. Esposito, A. Fuoco, J.C. Jansen, N.B. Mckeown, Redefining the Robeson upper bounds for CO2/CH4 and CO2/N2 separations using a series of ultrapermeable benzotriptycene-based polymers of intrinsic microporosity, Energy & Environmental Science. 12 (2019) 2733–2740. https://doi.org/10.1039/c9ee01384a.

[31] L. Robeson, Correlation of separation factor versus permeability for polymeric membranes. Journal of Membrane Science. 62 (1991) 165-185. https://doi.org/10.1016/037-7388(91)80060-J

[32] Y. Han, W.S. Winston Ho, Facilitated transport membranes for H_2 purification from coal-derived syngas: A techno-economic analysis. Journal of Membrane Science. 636 (2021) Article 119549. https://doi.org/10.1016/j.memsci.2021.119549

[33] O.I. Eriksen, E. Aksnes, I. M. Dahl, Facilitated transport of ethene through Nafion membranes. Part II. Glycerine treated, water swollen membranes. *Journal of Membrane Science,* 85 (1993) 99–106. https://doi.org/10.1016/0376-7388(93)85009-L

[34] M. Rungta, C. Zhang, W.J. Koros, L. Xu, Membrane-based ethylene/ethane separation: The upper bound and beyond, Aiche Journal. 59 (2013) 3475–3489. https://doi.org/10.1002/aic.14105.

[35] J. H. Kim, B. R. Min, H. S. Kim, J. Won, Y. S. Kang, Facilitated transport of ethylene across polymer membranes containing silver salt: effect of HBF4 on the photoreduction of silver ions. *Journal of Membrane Science,* 212 (2003) 283–288. https://doi.org/10.1016/S0376-7388(02)00451-9.

[36] A.C.C. Campos, R.A. Dos Reis, A. Ortiz, D. Gorri, I. Ortiz, A Perspective of Solutions for Membrane Instabilities in Olefin/Paraffin Separations: A Review, Industrial & Engineering Chemistry Research. 57 (2018) 10071–10085. https://doi.org/10.1021/acs.iecr.8b02013.

[37] J.P. Jung, C.H. Park, J.H. Lee, J.T. Park, J.-H. Kim, J.H. Kim, Facilitated olefin transport through membranes consisting of partially polarized silver nanoparticles and PEMA-g-PPG graft copolymer, Journal of Membrane Science. 548 (2018) 149-156. https://doi.org/10.1016/j.memsci.2017.11.020.

[38] Y. Zhao, W.S. Winston Ho, Steric hindrance effect on amine demonstrated in solid polymer membranes for CO_2 transport, Journal of Membrane Science. 415-416 (2012) 132-138. https://doi.org/10.1016/j.memsci.2012.04.044

[39] Y.R. Kim, J.H. Lee, H. Choi, W. Cho, Y.S. Kang, Chemical stability of olefin carrier based on silver cations and metallic silver nanoparticles against the formation of silver acetylide for facilitated transport membranes, Journal of Membrane Science. 463 (2014) 11-16. https://doi.org/10.1016/j.memsci.2014.03.057

[40] Y. Liu, X. Li, Y. Qin, R. Guo, J. Zhang, Pebax-polydopamine microsphere mixed-matrix membranes for efficient CO2separation, Journal of Applied Polymer Science. 134 (2017). https://doi.org/10.1002/app.44564.

[41] V.M. Kariuki, I. Yazgan, A. Akgul, A. Kowal, M. Parlinska, O.A. Sadik, Synthesis and catalytic, antimicrobial and cytotoxicity evaluation of gold and silver nanoparticles using biodegradable, Π-conjugated polyamic acid, Environmental Science: Nano. 2 (2015) 518–527. https://doi.org/10.1039/c5en00053j.

[42] J.G. Wijmans, R.W. Baker, The solution-diffusion model: a review, Journal of Membrane Science. 107 (1995) 1-21. https://doi.org/10.1016/0376-7388(95)00102-I

[43] W. Guo, T.N. Tran, H. Mondal, S. Schaefer, L. Huang, H. Lin, Superior CO2/N2 separation performance of highly branched Poly(1,3 dioxolane) plasticized by polyethylene glycol, Journal of Membrane Science. 648 (2022) 120352. https://doi.org/10.1016/j.memsci.2022.120352.

[44] L. Huang, J. Liu, H. Lin, Thermally stable, homogeneous blends of cross-linked poly(ethylene oxide) and crown ethers with enhance CO_2 permeability. Journal of Membrane Science. 610 (2020) Article 118252. https://doi.org/10.1016/j.memsci.2020.118253

[45] H. Lin, B. D. Freeman, Gas solubility, diffusivity, and permeability in poly(ethylene oxide). Journal of Membrane Science. 239 (2004) 105-117. https://doi.org/10.1016/j.memsci.2003.08.031

[46] J. Liu, G. Zhang, K. Clark, H. Lin, Maximizing Ether Oxygen Content in Polymers for Membrane CO2 Removal from Natural Gas, ACS Applied Materials & Interfaces. 11 (2019) 10933–10940. https://doi.org/10.1021/acsami.9b01079.

[47] Y. Li, M. Yavari, A. Baldanza, E. Di Maio, Y. Okamoto, H. Lin, M. Galizia, Volumetric Properties and Sorption Behavior of Perfluoropolymers with Dioxolane Pendant Rings, Industrial & Engineering Chemistry Research. 59 (2020) 5276–5286. https://doi.org/10.1021/acs.iecr.9b03411.

[48] M. van Essen, R. Thür, M. Houben, I. F.J. Vankelecom, Z. Borneman, K. Nijmeijer, Torturous mixed matrix membranes: A subtle balance between microporosity and compatibility, Journal of Membrane Science. 635 (2021) 119517. https://doi.org/10.1016/j.memsci.2021.119517

[49] S. Shahid, K. Nijmeijer, S. Nehache, I. Vankelecom, A. Deratani, D. Quemener, MOF-mixed matrix membranes: Precise dispersion of MOF particles with better compatability via a particle fusion approach for enhanced gas separation properties, Journal of Membrane Science. 492 (2015) 21-31. https://doi.org/10.1016/j.memsci.2015.05.015

[50] J.-J. Lin, W.-C. Tsai, Y.-C. Hsu, W.-H. Chang, Polymeric polyamines and method for stabilizing silver nanoparticle by employing the same, U.S. Patent 8013048B2, 2011.

[51] D.M. Muñoz, J.G. De La Campa, J. De Abajo, A.E. Lozano, Experimental and Theoretical Study of an Improved Activated Polycondensation Method for Aromatic Polyimides, Macromolecules. 40 (2007) 8225–8232. https://doi.org/10.1021/ma070842j.

[52] D. Kim, S. Jeong, J. Moon, Synthesis of silver nanoparticles using the polyol process and the influence of precursor injection, Nanotechnology. 17 (2006) 4019–4024. https://doi.org/10.1088/0957-4484/17/16/004.

[53] J. Schindelin, I. Arganda-Carreras, E. Frise, V. Kaynig, M. Longair, T. Pietzsch, S. Preibisch, C. Rueden, S. Saalfeld, B. Schmid, J.-Y. Tinevez, D.J. White, V. Hartenstein, K. Eliceiri, P. Tomancak, A. Cardona, Fiji: an open-source platform for biological-image analysis, Nature Methods. 9 (2012) 676–682. https://doi.org/10.1038/nmeth.2019.

[54] D.N. Benoit, H. Zhu, M.H. Lilierose, R.A. Verm, N. Ali, A.N. Morrison, J.D. Fortner, C. Avendano, V.L. Colvin, Measuring the Grafting Density of Nanoparticles in Solution by Analytical Ultracentrifugation and Total Organic Carbon Analysis, Analytical Chemistry. 84 (2012) 9238–9245. https://doi.org/10.1021/ac301980a.

[55] P. Larkin, *Infrared and Raman Spectroscopy: Principles and Spectral Interpretation*, Elsevier, 2017.

[56] R. M. Silverstein, F. X. Webster, D. J. Kiemle,, *Spectrometric Identification of Organic Compounds, 7th Edition*, Wiley, 2005.

[57] H. Günther, NMR Spectroscopy:Basic Principles, Concepts, and Applications in Chemistry, 3rd Edition, Wiley-VCH, 2013.

[58] B. A. Miller-Chou, J. L. Koenig, A review of polymer dissolution, Prog. Polym. Sci. 28 (2003) 1223-1270. https://doi.org/10.1016/S0079-6700(03)00045-5

[59] R.F. Fedors, A method for estimating both the solubility parameters and molar volumes of liquids, Polymer Engineering & Science. 14 (1974) 147–154. https://doi.org/10.1002/pen.760140211.

[60] B. Buszewski, K. Rafiłska, P. Pomastowski, J. Walczak, A. Rogowska, Novel aspects of silver nanoparticles functionalization, *Colloids and Surfaces A: Physicochemical and Engineering Aspects.* 506 (2016) 170–178. https://doi.org.10.1016/j.colsurfa.2016.05.058.

[61] H. Sigel, R.B. Martin, Coordinating properties of the amide bond. Stability and structure of metal ion complexes of peptides and related ligands, Chemical Reviews. 82 (1982) 385–426. https://doi.org/10.1021/cr00050a003.

[62] J.H. Lee, S.W. Kang, M.S. Yeom, Y.R. Kim, H. Choi, D. Song, J. Won, Y.S. Kang, A strong linear correlation between the surface charge density on Ag nanoparticles and the amount of propylene adsorbed, Journal of Materials Chemistry A. 2 (2014) 6987. https://doi.org/10.1039/c4ta00026a.

[63] R.G. Shimmin, A.B. Schoch, P.V. Braun, Polymer Size and Concentration Effects on the Size of Gold Nanoparticles Capped by Polymeric Thiols, Langmuir. 20 (2004) 5613–5620. https://doi.org/10.1021/la036365p.

[64] Z. Farashi, S. Azizi, M. Rezaei-Dasht Arzhandi, Z. Noroozi, N. Azizi, Improving CO_2/CH_4 separation efficiency of Pebax-1657 membrane by adding Al_2O_3 nanoparticles in its matrix, Journal of Natural Gas Science and Engineering. 72 (2019) Article 10319. https://doi.org/10.1016/j.jngse.2019.103019

[65] M. Isanejad, N. Azizi, T. Mohammadi, Pebax membrane for CO2 /CH4 separation: Effects of various solvents on morphology and performance, Journal of Applied Polymer Science. 134 (2017). https://doi.org/10.1002/app.44531.

[66] W.J. Box, M.T. Webb, M. Galizia, Evaluating the Experimental Uncertainty in Gas and Vapor Sorption/Adsorption Measurements: Fundamental Considerations and Experimental Design Implications, Industrial & Engineering Chemistry Research. 61 (2022) 9856–9868. https://doi.org/10.1021/acs.iecr.2c01414.

[67] L. M. Robeson, The upper bound revisited, Journal of Membrane Science, 320 (2008), 390-400. https://doi.org/10.1016/j.memsci.2008.04.030

[68] K. Ghosal, R.T. Chern, B.D. Freeman, W.H. Daly, I.I. Negulescu, Effect of Basic Substituents on Gas Sorption and Permeation in Polysulfone, Macromolecules. 29 (1996) 4360–4369. https://doi.org/10.1021/ma951310i.

[69] C.S.K. Achoundong, N. Bhuwania, S.K. Burgess, O. Karvan, J.R. Johnson, W.J. Koros, Silane Modification of Cellulose Acetate Dense Films as Materials for Acid Gas Removal, Macromolecules. 46 (2013) 5584–5594. https://doi.org/10.1021/ma4010583.

[70] C.T. Wright, D.R. Paul, Gas sorption and transport in UV-irradiated poly(2,6-dimethyl-1,4-phenylene oxide) films, J. Appl. Polym. Sci. 67(5) (1998) 875-883. https://doi.org/10.1002/(SICI)1097-4628(19980131)67:5<875::AID-APP13>3.0.CO;2-N

[71] T. C. Merkel, R. Blanc, I. Ciobanu, B. Firat, A. Suwarlim, J. Zeid, Silver salt facilitated transport membranes for olefin/paraffin separation: Carrier instability and a novel regeneration method, Journal of Membrane Science, 447 (2013) 177-189. https://doi.org/10.1016/j.memsci.2013.07.010